COMSOL
CONFERENCE
2024 BOSTON

Mxene Doped Perovskite Solar Cell Simulation for Enhanced Efficiency

Kevin Gurbani Beepat[1], Davinder Pal Sharma[1], Aman Mahajan[2], Dinesh Pathak[1], Vinod Kumar[1]
1. Department of Physics, University of the West Indies, St. Augustine, Trinidad and Tobago.
2. Department of Physics, Guru Nanak Dev University, Amritsar, India.

Abstract
The incorporation of two dimensional MXenes with perovskite solar cells have garnered much attention in recent years. MXenes of the form $Ti_3C_2T_x$ have shown unique electrical capabilities due to its surface terminating functional group T_x. Additionally, the inclusion of this material to perovskite solar cells has resulted in enhanced efficiency and improved optoelectronic performances. In the present work, COMSOL Multiphysics was used to simulate MXene doped perovskite solar cells consisting of an electron transport layer (ETL), absorber layer consisting of perovskite ($MAPbI_3$) and Mxene ($Ti_3C_2T_x$) and hole transport layer (HTL) with a configuration ETL/ $MAPbI_3$ + MXene/ HTL. For the materials, TiO_2 (120 nm) was used as the ETL and Spiro-OMeTAD (140 nm) was used as the HTL. The impact of both thickness and concentration of the absorber layer ($MAPbI_3$ + MXene) were thoroughly studied to boost its efficiency. The ideal variation in thickness and doping concentration was then used to inform the design of an optimal solar cell structure which achieved a maximum efficiency of 19.87%, a fill factor of 0.57, open-circuit voltage (V_{OC}) of 1.10V and short circuit current density (J_{SC}) of 31.97 mA/cm^2. To the best of our knowledge, this is the first time COMSOL Multiphysics was used to simulate perovskite solar cells doped with 2D $Ti_3C_2T_x$ MXene. The results therefore give meaningful guidance and insight into the fabrication and further study of MXene doped perovskite solar cells.

Keywords: Perovskite, MXene, COMSOL, Simulation.

Introduction
Perovskite solar cells have garnered much attention in recent years due to their low cost, high performance and solution processability [1] as well as their tunability and optical absorption [2]. So far, perovskite solar cells have achieved a maximum efficiency of 25.8% as reported by Min et. al. [3]. However, there is much room for improvement as its stability and efficiency can be further enhanced [4]. Additionally, MXene doped perovskite solar cells have scarcely been researched and therefore has great potential for improving its performance.

Perovskite solar cells are usually built in a sandwich structure accompanied by an electron transport layer (ETL) and a hole transport layer (HTL). These layers are important for the overall performance of the solar cell since the ETL has a high electron mobility and low hole mobility which is therefore suitable to transport electrons away from the absorber layer and toward the electrodes [5]. Similarly, the HTL has a high hole mobility and low electron mobility which makes it appropriate to carry holes away from the absorber layer and toward the electrodes [6].

Additionally, MXenes are a family of two dimensional transition metal carbides, nitrides and carbononitrides with high electrical conductivity as well as tunable and hydrophilic surfaces [7]. MXenes in solar cells and Mxene doped perovskite solar cells have rarely been research and as far as we know, this research presents the first time MXene doped solar cells have never been simulated. In 2011, when looking for a path to insert lithium ions in layers of ternary transition metal carbide or nitride phases, it was found that the aluminium (Al) layers can be selectively removed by immersing Ti_3AlC_2 particles in hydrofluoric acid. This reduced the bulk three dimensional structure of Ti_3AlC_2 into two dimensional Ti_3C_2 layers where the surface titanium atoms (Ti) are terminated with groups such as –O, -F and –OH [7]. In the formula, Ti is referred to as T which gives the formula for the MXene layer as $Ti_3C_2T_x$. in general, MXenes have the formula $M_{n+1}X_nT_x$ where M denotes an early transition metal, X is a carbon/ nitrogen atom and T represents the surface termination group [8]. Due to its tunable termination group MXenes exhibit a wide variety of optical and electrical properties which has great potential to impact the photovoltaic space.

Additionally, perovskite is a photo-sensitive material that is able to generate electrons and holes when photons are incident on it. Perovskite solar cells are among the fastest advancing solar cell technology. It has a crystal structure of $CH_3NH_3PbX_3$ where X can be an I, Br or Cl atom [2]. Hence, it is common to abbreviate the methylammonium ion ($CH_3NH_3^+$) to MA as is done in this paper. Also, $MAPbI_3$ has an optical bandgap between 1.55 – 2.3 eV depending on the halide content [2].

COMSOL Multiphysics uses the Finite Element Method (FEM) to numerically solve its partial

difference equations. FEM involves dividing the domain, in this case the sandwich heterostructure of the solar cell, into numerous subdomains called finite elements which are linked together by nodes. The method then involves seeking continuous polynomial solutions over each element in terms of nodal values, assembling the element equations into a global matrix using interelement continuity and the balance of the interelement forces [9]. When the finite elements are applied to a geometry, it is called a mesh. The mesh is used to approximate the structure and the quality of the mesh is one of the determining factors for the quality of the results [10]. Therefore, although the FEM is a powerful numerical tool, it is important that its governing equations, boundary conditions and mesh are applied appropriately to ensure accurate convergence on a solution.

Additionally, a solar cell's efficiency is limited by heating effects that occur when current passes through it. Joule heating [11] and nonradiative recombination heating [12] are the sources of these heating effects. Every time a current flows through a resistive material—in this case, the semiconductor material—joule heating occurs [11]. Furthermore, when electrons enter trap states that are present within the semiconductor's band gap, nonradiative recombination heating occurs. It is dubbed nonradiative because these sites offer an alternate route for electrons to recombine, resulting in no photons being generated. Instead, thermal energy is released in the form of phonons [13]. This process needs to be limited because it may reduce the solar cell's efficiency.

In this work, a MXene doped perovskite solar cell is numerically solved with the configuration ETL (TiO_2)/ $MAPbI_3$ + MXene ($Ti_3C_2T_x$)/ HTL (Spiro-OMeTAD) in order to study and improve its efficiency. The influence of both the thickness and doping concentration of the absorber were carefully studied. Additionally, the generation/ recombination of charge carriers, internal heating mechanisms and energy band diagrams of the solar cell were also studied.

Theory

To get results, COMSOL Multiphysics applies the FEM to the continuity equations, drift diffusion equation, Poisson equation, and photogeneration equation with appropriate boundary conditions. The simulations relied on the solar spectrum as shown in Figure 1.

The photogeneration equation applied is given by

$$G(z) = \int_0^\infty \alpha(\lambda)\phi(\lambda)\exp(-\alpha(\lambda)z)d\lambda \quad (1)$$

where z is the device's distance from the surface, λ is the wavelength, and α(λ) denotes the absorption coefficient described by

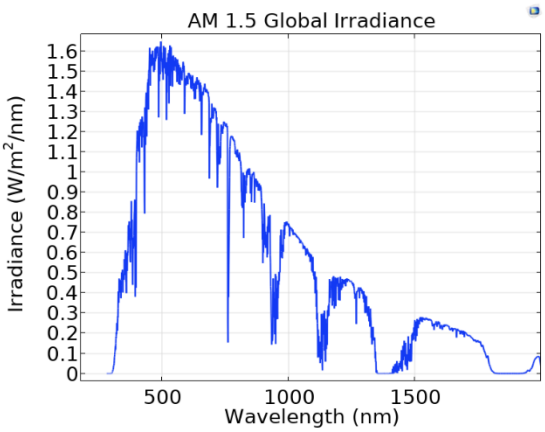

Figure 1. Solar spectrum used in simulations [14] [15].

$$\alpha(\lambda) = \frac{4\pi\kappa(\lambda)}{\lambda} \quad (2)$$

where κ(λ) is the imaginary part of the refractive index of the material and ϕ(λ) is the photon generation rate defined by

$$\phi(\lambda) = \frac{\lambda}{hc}F(\lambda) \quad (3)$$

where F(λ) is the spectral irradiance approximated to be AM 1.5 and shown in Figure 1. The Poisson equation is given by

$$\nabla \cdot (-\epsilon_0\epsilon_r\nabla V) = \rho \quad (4)$$

where ϵ_0 is the permittivity of free space and ϵ_r is the relative permittivity of the material. V is the electric potential and ρ is the charge density given by

$$\rho = q(p - n + N_D^+ - N_A^-) \quad (5)$$

Where q the electric charge of an electron is, p is the density of holes and n is the density of electrons. N_D^+ and N_A^- is the donor doping and acceptor doping concentrations. The variables n and p are given by

$$n = N_c exp\left(\frac{q(E_{f_0} - E_c)}{k_b T}\right) \quad (6)$$

$$p = N_v exp\left(\frac{q(E_v - E_{f_0})}{k_b T}\right) \quad (7)$$

Where N_c and N_v are the conduction band and valence band density of states respectively, E_c, E_v and E_{f_o} is the conduction band, valence band and fermi energy levels respectively and T is the temperature. The drift diffusion equations are therefore

$$J_n = qn\mu_n\nabla E_c + qD_n\nabla n - qnD_n\nabla \ln(N_c) + qnD_n\nabla \ln(T) \quad (8)$$

$$J_p = qp\mu_p \nabla E_v + qD_p \nabla \mathrm{p} - qpD_p \nabla \ln(N_v) + qpD_p \nabla \ln(T) \quad (9)$$

Where $D_{n,p} = \mu_{n,p} k_b T$. Applying these equations to the geometry and using a suitable mesh and boundary conditions allows for an accurate construction of the problem while leads to reliable results.

Methods

In this study the geometry of the sandwich structure was built in one dimension with a cross-sectional area of 1 cm^2 as shown in Figure 2. The material properties such as the bandgap energy, electron/ hole mobilities and carrier lifetimes were then added as shown in Table 1. The physics of the simulation was then added using the *Semiconductor Module*. Here, the electrode contacts, the doping profiles, the trapping mechanisms and the generation mechanisms were applied. For this study, Shockley-Read-Hall (SRH) recombination was applied, and the carrier generation was applied according to equation 1. Next, the mesh was applied to the geometry consisting of an edge mesh of 50 elements for each segment. The mesh was given a geometric distribution so that at the junctions there would be more elements than in the centre. This was done to help capture more detail in the simulation. Finally, the study was done in two stages. The first was a *semiconductor equilibrium* study where the continuity parameter was ramped up to 1. This aided in achieving convergence. The second step involved a *stationary study* where a voltage sweep from 0 – 1V was done. The JV, thermal, energy level diagrams and generation recombination graphs were produced and studied to better understand the behaviour of the solar cell.

Additionally, the experiment was repeated two times, the first by changing the thickness of the $MAPbI_3$ + MXene ($Ti_3C_2T_x$) absorber layer from 200 nm to 500 nm and next by changing the doping concentration of the absorber layer from $1 \times 10^{12} cm^{-3}$ to $1 \times 10^{16} cm^{-3}$. The optimal thickness of 500 nm and doping concentration of 1×10^{15} cm^{-3} was then applied to study the results of an optimised solar cell.

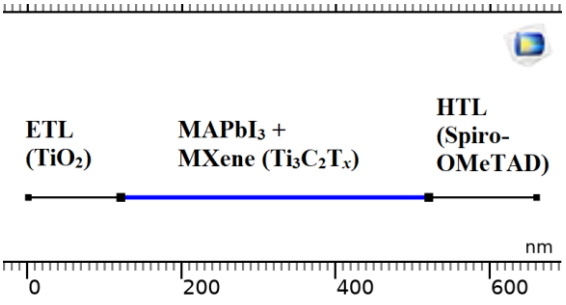

Figure 2. Geometry used in simulations.

Table 1. *Parameters of the materials used in the simulations.*

Parameters	**TiO_2** [16]	**$MAPbI_3$ + MXene ($Ti_3C_2T_x$)** [16]	**Sprio-OMeTAD** [16]
Thickness (nm)	**120**	**450**	**140**
Bandgap (V)	**3.2**	**1.6**	**3**
χ (V)	**3.95**	**3.55**	**2.2**
ε_r	**100**	**6.5**	**3**
N_c (cm^{-3})	**2.2×10^{18}**	**1×10^{19}**	**2.2×10^{18}**
N_v (cm^{-3})	**1.8×10^{19}**	**1×10^{19}**	**1.8×10^{19}**
μ_n (cm^2/Vs)	**0.02**	**2**	**5×10^{-3}**
μ_p (cm^2/Vs)	**2**	**2**	**2×10^{-3}**
N_A (cm^{-3})	**0**	**9×10^{15}**	**3×10^{16}**
N_D (cm^{-3})	**9×10^{17}**	**0**	**0**
τ_n (ns)	**6**	**8**	**6**
τ_p (ns)	**0.1**	**1**	**1**

Results & Discussion

Changing thickness of absorber layer

The first study conducted involved changing the thickness of the absorber layer with the resulting JV graph shown in Figure 3. From the graph it can be seen that by increasing the thickness of the absorber layer, the open circuit voltage (V_{OC}) remains fairly constant at around 1.13V while the short circuit current density (J_{SC}) increased from 20.56 mA/cm^2 to 30.00 mA/cm^2.

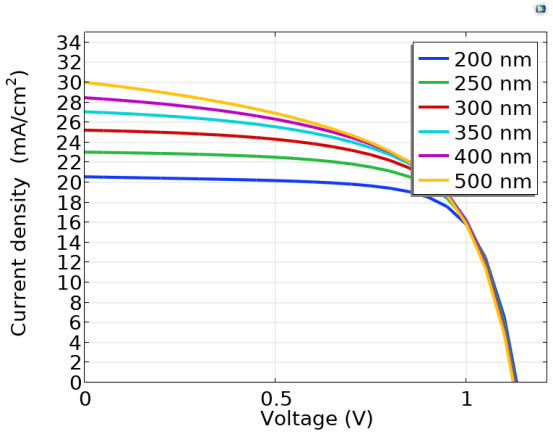

Figure 3. Varying thickness of the absorber layer.

This change is indicative of a decrease in the series resistance of the solar cell brought about by increasing the thickness of the absorber layer. By increasing the thickness, there is enhanced light

absorption and therefore greater generation of charge carriers. Therefore, more charge carriers can reach the electrode contacts, effectively lowering the resistance of the solar cell.

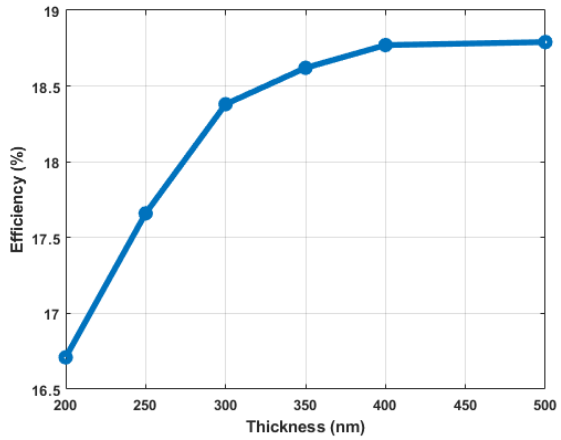

Figure 4. Efficiency vs. Thickness of the absorber layer.

Figure 4 shows the relationship between the efficiency of the solar cell and the thickness of the absorber layer. As expected with a decreasing series resistance, the efficiency increases as the thickness of the absorber layer increases. We can also see that from around 400 nm the efficiency increase saturates meaning that recombination processes begin to dominate which prevents further increase in the efficiency. Similarly, Figure 5 shows that increasing the thickness of the absorber layer leads to a decrease in the Fill Factor (FF) of the solar cell since the change in J_{SC} is large compared to the change in V_{OC}. This is further highlighted in both Figure 6 and Figure 7.

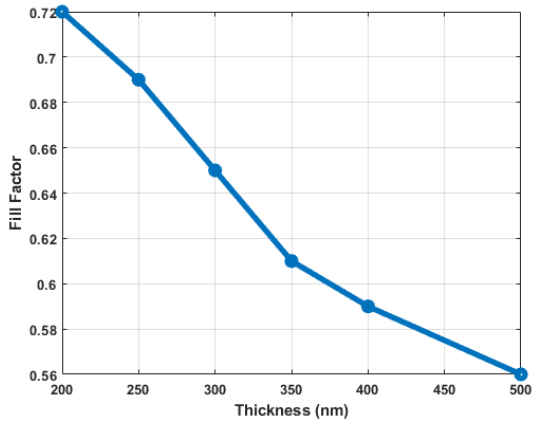

Figure 5. Fill Factor vs. thickness of the absorber layer.

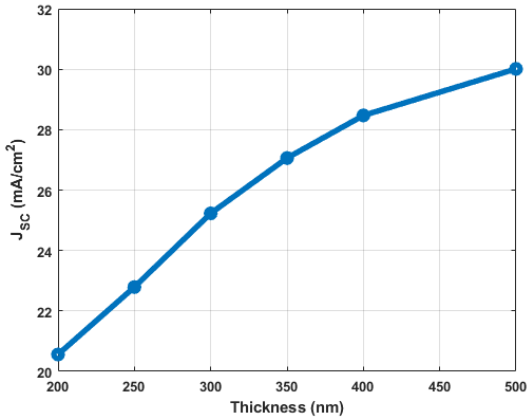

Figure 6. J_{SC} vs. thickness of the absorber layer.

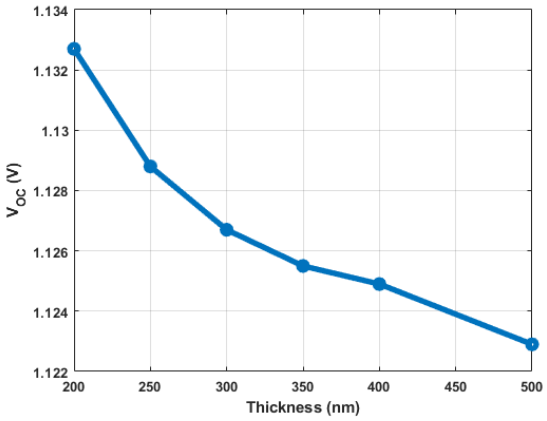

Figure 7. V_{OC} vs. thickness of the absorber layer

Changing doping concentration of absorber layer

The second study conducted involved changing the doping concentration of the absorber layer and studying its effects. From Figure 8 it can be seen that by increasing the doping concentration of the absorber layer from $1 \times 10^{12}\text{cm}^{-3}$ to $1 \times 10^{16}\text{cm}^{-3}$ there was little change to the JV graph apart for the $1 \times 10^{16}\ \text{cm}^{-3}$ doping concentration. This can be explained by the fact that although there was an increase in the doping concentration and therefore more charge carriers, the recombination processes dominated which limited the potential for increasing the efficiency.

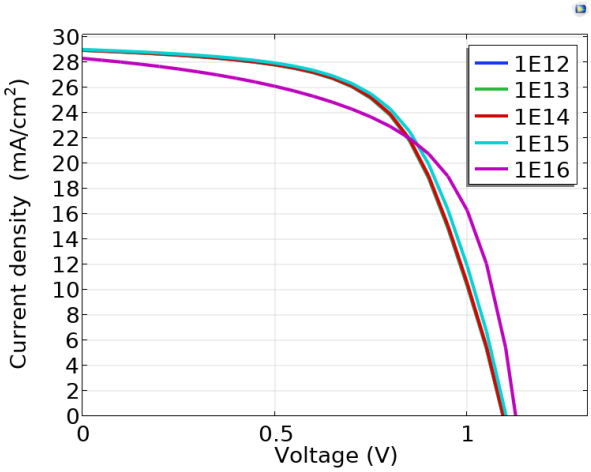

Figure 8. Varying doping concentration of the absorber layer.

This can be further seen in Figure 9 which shows the change in efficiency when the doping concentration is increased. From the graph it can be seen that by increasing the doping concentration there is an initial increase in efficiency since more charge carriers are available to deliver current to the electrodes. However, there is a sharp fall in efficiency after 1×10^{15} cm^{-3}. This drop in efficiency is due to the fact that by increasing the doping concentration too much there are too many charge carriers present and recombination processes begin to dominate.

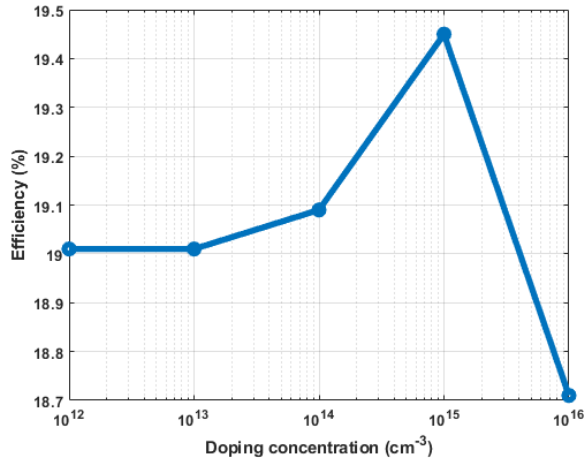

Figure 9. Efficiency vs. doping concentration of the absorber layer.

This point is further highlighted in Figure 10 and Figure 11 where an increasing doping concentration also increased the Fill Factor and J_{SC} values respectively until recombination takes over and therefore experiences a sharp decrease at a doping concentration of $1 \times 10^{16} cm^{-3}$. However, in Figure 12 it can be seen that by increasing the doping concentration of the absorber layer also leads to an increase in the V_{OC}. This is due to the fact that increasing the doping concentration also increases the built-in voltage which means that more voltage is required to overcome it and allow a current to pass. Therefore, the V_{OC} increases with increasing doping concentration.

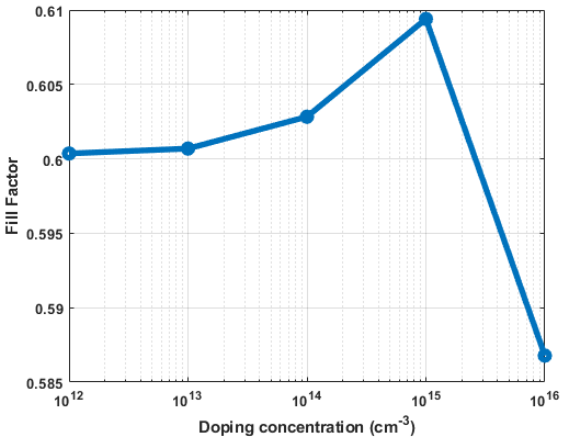

Figure 10. Fill Factor vs. doping concentration of the absorber layer.

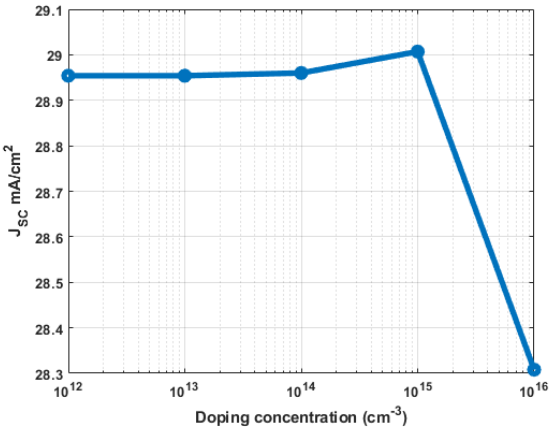

Figure 11. J_{SC} vs. doping concentration of the absorber layer.

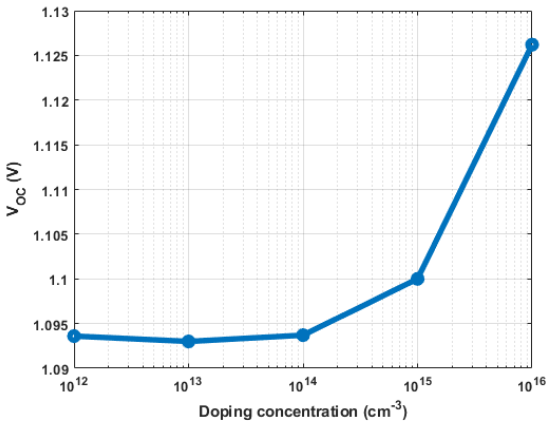

Figure 12. V_{OC} vs. doping concentration of the absorber layer.

Optimised solar cell

By analysing the results of changing the thickness of the absorber layer as well as changing the doping concentration of the absorber layer it was determined

that 500 nm was the optimal thickness of the absorber layer and $1 \times 10^{15} cm^{-3}$ was the ideal doping concentration. Therefore, when the simulation was repeated with these parameters the resultant efficiency was 19.87% as shown in Figure 13 and summarised in Table 2.

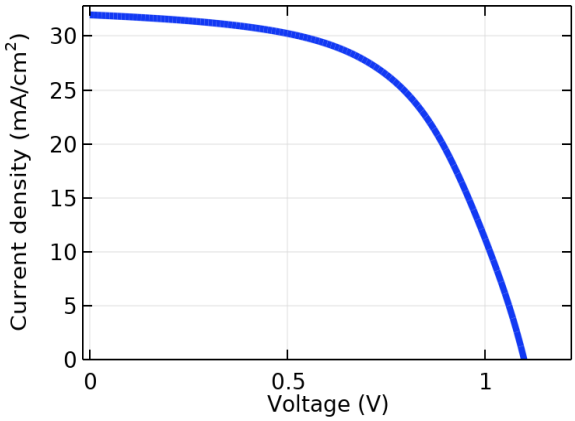

Figure 13. JV graph of optimised solar cell.

Table 2. *J_{SC}, V_{OC}, FF and efficiency of optimised solar cell.*

J_{SC} (mA/cm²)	V_{OC} (V)	FF	Efficiency (%)
31.97	1.10	0.57	19.87

Additionally, Figure 14 shows the energy level diagram for the solar cell with the flow of electrons and holes.
The generation/ recombination of charge carriers as well as the heating effects within the solar cell were also analysed. From Figure 15 it can be seen that most of the generation of the charge carriers occur at the beginning of the cell where photons are incident. On the other hand recombination occurs at three main sites, namely the middle of each layer.

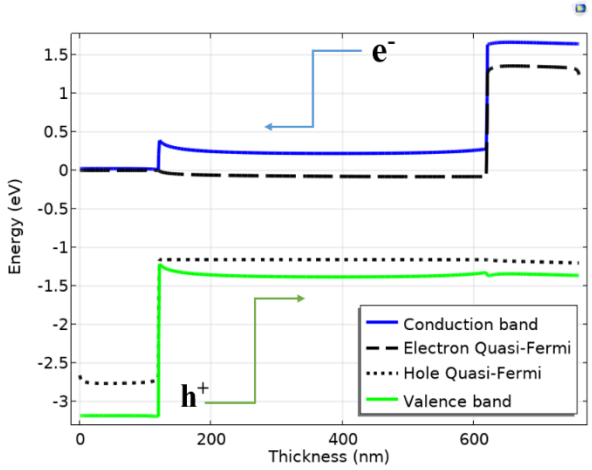

Figure 14. Energy level diagram for optimised solar cell.

This is expected since it is at these sites that most of the charge carriers are present for recombination. The sites of the recombination also explains why in Figure 16 most of the nonradiative recombination heating occurs at the same locations.

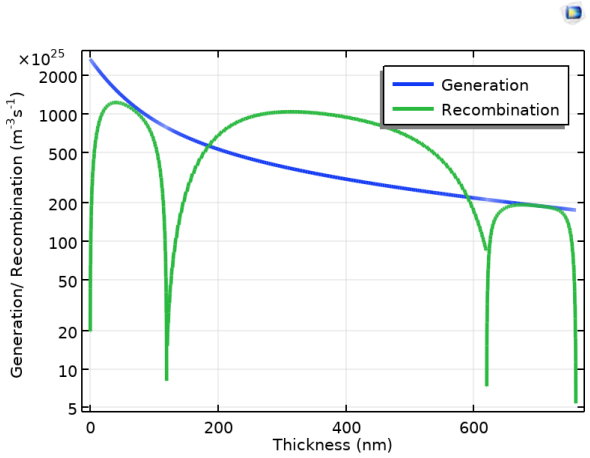

Figure 15. Generation/ Recombination graph of optimised solar cell.

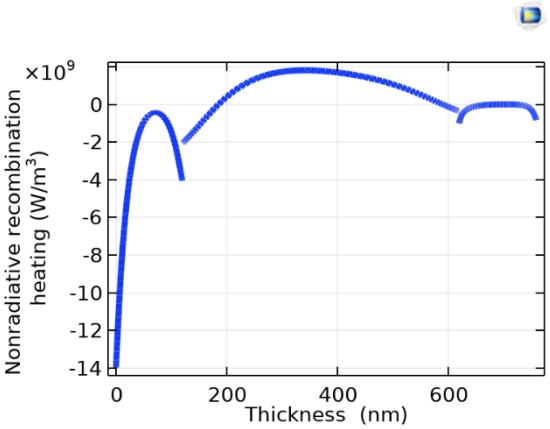

Figure 16. Nonradiative recombination heating within optimised solar cell.

Additionally, Figure 17 shows the site of Joule heating which is at the first junction of the solar cell where the absorber layer starts.

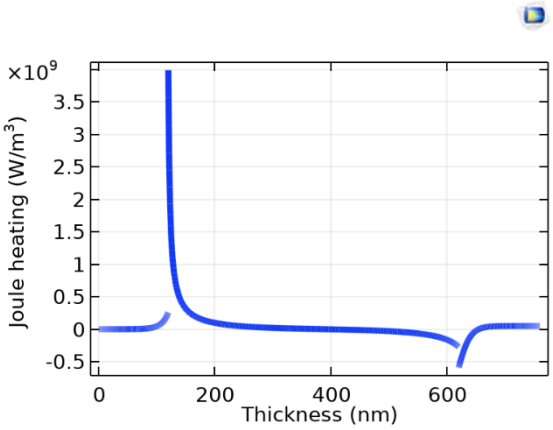

Figure 17. Joule heating within optimised solar cell.

Since Joule heating arises from the flow of charges, it follows then that the site of most Joule heating will correspond with the location of the absorber layer.

It should also be noted that there are ways to further extend this research. For example, the study can be repeated using two and three dimensional geometries. Additionally, experimental results can be used to compare the results of this study.

Conclusions

COMSOL Multiphysics was used to simulate MXene doped perovskite solar cells consisting of an electron transport layer (ETL), absorber layer consisting of perovskite ($MAPbI_3$) and MXene ($Ti_3C_2T_x$) and hole transport layer (HTL) with a configuration ETL/ $MAPbI_3$ + MXene/ HTL. TiO_2 was used as the ETL and Spiro-OMeTAD was used as the HTL. The impact of both thickness and doping concentration of the absorber layer were numerically studied and it was found that the ideal thickness for the absorber layer was 500 nm and the optimal doping concentration of the absorber layer was 1×10^{15} cm^{-3}. This was then applied to the design of an optimal solar cell structure which achieved a maximum efficiency of 19.87%, a fill factor of 0.57, open-circuit voltage (V_{OC}) of 1.10V and short circuit current density (J_{SC}) of 31.97 mA/cm^2. The heating profile of the solar cell caused by both Joule heating and nonradiative recombination heating were also studied and it was found that the Joule heating mostly occurred where the absorber layer started whereas the nonradiative recombination occurred in the midsection of each layer. Additionally, the generation/ recombination of charge carriers were also studied and it was found that the generation of charge carriers occurred where photons were incident whereas the recombination occurred in each layer. The results of this study can be used to help guide the construction and further research of MXene based perovskite solar cells.

References

[1] B. Abdulaziz and L. Y. Zhong, "Next-generation applications for integrated perovskite solar cells.," *Communications Materials*, vol. 4, no. 2, 2023.

[2] K. Beepat and S. Kumar, "Perovskite materials for photovoltaics: a review," *The European Physical Journal Applied Physics*, 2023.

[3] H. Min and D. Y. Lee, "Perovskite solar cells with atomically coherent interlayers on SnO2 electrodes," *Nature*, pp. 444-450, 2021.

[4] T. Chowdhury and M. Zafar, "Stability of perovskite solar cells: issues and prospects," *Royal Society of Chemisty*, pp. 1787-1810, 2023.

[5] S. Foo and M. Thambidurai, "Recent review on electron transport layers in perovskite solar cells," *International Journal of Energy Research*, pp. 21441-21451, 2022.

[6] K. Anoop and T. Ahipa, "Recent advancements in the hole transporting layers of perovskite solar cells," *Solar Energy*, p. 111937, 2023.

[7] B. Anasori and M. Naguib, "Two-dimensional MXenes," *MRS Bulletin*, pp. 238-244, 2023.

[8] H. Song and T. Nguyen, "Nanotechnology in the automotive industry," *Micro & Nano Technology Series*, pp. 485-504, 2022.

[9] J. N. Reddy, An introduction to the Finite Element Method, 2003.

[10] A. Kulkarni and V. Havanur, Finite Element Analysis, 2014.

[11] E. Yandri and N. Hagino, "Joule Heating Estimation of Photovoltaic Module Through Cells Temperature Measurement," *International Journal of Power Electronics and Drive Systems*, pp. 1119-1128, 2022.

[12] V. M. Agranovich and A. A. Maradudin, Nonradiative recombination in semiconductors, Elsevier, 1991.

[13] I. Lashkevych, O. Titov and Y. G. Gurevich, "Recombination and temperature distribution in semiconductors," *Semiconductor Science and Technology*, p. 055014, 2012.

[14] C. Wehrli, " Extraterrestrial Solar Spectrum," *Physikalisch-Meteorologisches Observatorium + World Radiation Center*, 1985.

[15] H. Neckel and D. Labs, "Improved Data of Solar Spectral Irradiance from 0.33 to 1.25 µm," *Solar Physics*, 1981.

[16] S. K. Azadi and S. Asgharizadeh, "Comparative performance analysis of HTLs in MXene-assisted perovskite solar cells," *Optics Communications*, p. 129104, 2023.